17th AIAA/CEAS Aeroacoustics Conference (32nd AIAA Aeroacoustics Conference)
05 - 08 June 2011, Portland, Oregon

AIAA 2011-2713

Experimental assessment of the noise generated at the leading edge of porous airfoils using microphone array techniques

Thomas Geyer* Ennes Sarradj† Jens Giesler* Marcus Hobracht‡

Aeroacoustics Group, Brandenburg University of Technology, 03046 Cottbus, Germany

The use of flow–permeable materials is a known method for the reduction of airfoil aeroacoustic noise. Detailed acoustic measurements on the noise generation at the leading edge of porous airfoil models were performed in an open jet wind tunnel using microphone array measurement techniques and three–dimensional beamforming algorithms. A set of three different grids provided the required inflow turbulence. Measurement results are presented for the noise generated at the leading edge of porous airfoils, which are characterized by their air flow resistivity, compared to a non–porous reference airfoil. The comparison of the leading edge noise spectra measured for the reference airfoil with theory yields good agreement. The results of the acoustic measurements show that porous airfoils with low air flow resistivities lead to a noticeable noise reduction, which is assumed to be caused by the larger pores of these materials compared to porous airfoils with a higher air flow resistivity.

Nomenclature

a	bar width or rod diameter of the grid [m]	$R(\tau)$	autocorrelation function
A_s	cross–sectional area of porous sample [m^2]	Re	Reynolds number
b	hole diameter of the grid [m]	SPL	sound pressure level [dB]
B, C	constant factors	Sr	Strouhal number
c	speed of sound [m/s]	t	grid thickness [m] or time [s]
c_l	chord length [m]	Tu	turbulence intensity [%]
d_s	thickness of porous sample [m]	u	turbulent velocity fluctuations [m/s]
f	frequency [Hz]	u_s	static fluid flow through porous sample [m/s]
f_c	center frequency [Hz]	U	mean flow velocity [m/s]
h	airfoil semi–span [m]	U_0	nominal flow speed [m/s]
K_x	chordwise turbulence wavenumber	x, y, z	cartesian coordinates
M	mesh width [m]		
Ma	mean flow Mach number	β	grid porosity
n	scaling exponent	λ	acoustic wavelength [m]
Δp_s	pressure difference [Pa]	Λ	integral length scale [m]
r	air flow resistivity [Pa s/m^2]	ν	kinematic viscosity [m^{2}s^{-1}]

I. Introduction

When an airfoil is subject to a turbulent inflow, the aeroacoustic noise is dominated by sound generated at the leading edge of the airfoil. This leading edge noise is a result of turbulent structures which generate fluctuating forces that act on the airfoil. Leading edge noise is therefore assumed to be strongly dependent on the characteristics of the inflow turbulence. In general, two different cases may be considered:[1] When

*Research Assistant, Aeroacoustic Modeling and Optimization, BTU Cottbus, Siemens-Halske-Ring 14, 03046 Cottbus.
†Junior Professor, Aeroacoustic Modeling and Optimization, BTU Cottbus.
‡Master Student, Aeroacoustic Modeling and Optimization, BTU Cottbus.

the characteristic scale of the turbulent eddies is not small with respect to the chord length of the airfoil, the total aerodynamic load of the airfoil is affected and noise is generated in a range of low frequencies. When the scale of the eddies is much smaller than the dimensions of the airfoil, the eddies are deformed when they impinge on the airfoil leading edge, leading to local changes of the aerodynamic load and an emission of noise at high frequencies.

A fundamental work on the noise from an airfoil subject to a turbulent flow was performed by Amiet,[2] who states that, basically, the noise generated at an airfoil in a turbulent flow is directly related to the unsteady loading of the airfoil. He developed a noise prediction model by taking into account the cross-power spectral density of the surface pressure on the airfoil due to the inflow turbulence characterized by its energy spectrum. The part of the resulting model which applies to the high–frequency range allows for the calculation of the third–octave band far field sound pressure level (SPL) based on the airfoil semi–span h, the Mach number $Ma = U/c$, the integral length of the turbulence Λ and the intensity of the turbulence $\sqrt{\overline{u^2}}/U$:

$$SPL = 10 \cdot \log_{10}\left(\frac{\Lambda \cdot h}{z^2} \cdot \left(\frac{U}{c}\right)^5 \cdot \frac{\overline{u^2}}{U^2} \cdot \frac{\hat{K}_x^3}{(1+\hat{K}_x^2)^{7/3}}\right) + 181.3 \text{ dB}. \tag{1}$$

In Equation (1), $K_x = \omega/U$ is the chordwise turbulence wavenumber (which is normalized by the wavenumber range of the energy containing eddies, denoted by the $\wedge$ symbol) and z is the observer distance normal to the airfoil. The model includes a dependence on the fifth power of the Mach number and on the square of the turbulence intensity. The predicted third–octave band sound pressure levels show reasonable agreement with data measured on a flat plate in an anechoic wind tunnel.

Paterson and Amiet[3] performed acoustic measurements on a NACA 0012 airfoil in an open jet wind tunnel. A square mesh grid generated nearly isotropic incident turbulence with a turbulence intensity in the order of 4% to 5%, and hence the leading edge was identified as the dominant noise source region, resulting in the generation of broadband noise. Besides the acoustic measurements, hot–wire measurements were conducted to characterize the turbulence, which was found to be approximately homogeneous and, to some extent, anisotropic. Good agreement between the measured leading edge noise in comparison to the noise predicted by the model of Amiet[2] at low frequencies and for high Mach numbers was observed. Paterson and Amiet state that a potential way to reduce airfoil leading edge noise may be the reduction of the ratio of turbulence scale to airfoil thickness.

Airfoil leading edge noise is a major noise source that may exceed the trailing edge noise to a large extent (see for example the work by Sharland[4]), which clearly emphasizes the demand for a reduction of this noise source. Besides the possibility to choose airfoil designs that are known to generate less leading edge noise than others, as for example thick airfoils with large leading edge radii rather as opposed to thin airfoils, there exist several concepts for the reduction of airfoil leading edge noise by means of flow permeable materials.

For example, Lee[5] performed a numerical investigation on the leading edge noise generated at a porous helicopter blade and found that a noticeable reduction of the far field noise is possible. According to this study, the physical mechanism responsible for the noise reduction is the suppression of pressure fluctuations near the leading edge.

A computational study on the reduction of wake-stator-interaction noise using airfoils with a plenum chamber under a porous surface section in a subsonic flow field was done by Tinetti et al.[6] Reductions of the peak level in the order of 1 dB were observed. In general, the attenuation of the radiated noise was related to the reduction of the amplitudes of the pressure peaks at the surface caused by the porosity.

The results of a past experimental study on the reduction of airfoil trailing edge noise by means of completely porous airfoils[7,8] are very encouraging and show the considerable potential of open porous materials for aeroacoustic noise reduction.

The present paper introduces an experimental study on the leading edge noise reduction that can be achieved through the use of such airfoils made of an open porous material. The required inflow turbulence is generated through a set of three turbulence grids that are mounted to the nozzle of an open jet wind tunnel. The intention of the present study is the identification of differences regarding the noise generation at the leading edge of porous airfoils in a subsonic stream to a non–porous reference airfoil of similar geometry. Thereby, the focus of this paper is on the measurement of the airfoil leading edge noise (the measurement setup, especially the turbulence generating grids, and the data processing techniques), and consequently the results are presented briefly only. However, the measured leading edge noise spectra may then be used for the development of a leading edge noise model for porous airfoils.

II. Materials and methods

To investigate the influence of the material parameters of a set of porous airfoils on the generation of noise at the airfoil leading edge at zero angle of attack, acoustic measurements were performed in the small aeroacoustic wind tunnel at the Brandenburg University of Technology in Cottbus. The inflow turbulence required to generate noise at the leading edge of an airfoil was generated by the use of grids. The acoustic measurements were performed using advanced microphone array technology and three–dimensional beamforming algorithms.

II.A. Airfoil models

Measurements were conducted on a set of 16 porous airfoils and a non–porous reference airfoil with a chord length of 235 mm and a span width of approximately 400 mm. While the reference airfoil has an SD7003 shape[9] with a trailing edge thickness of 0.5 mm, the shape of the porous airfoils is basically the same SD7003 shape, but with a slightly increased trailing edge thickness of 1.59 mm to enable the manufacturing of the airfoils out of the different porous materials. Due to the past study of trailing edge noise, the reference airfoil is additionally equipped with a thin tripping tape at 10.6% of the chord, which was not removed for the present study. However, regarding the shape and dimension of the leading edge, the porous airfoils and the reference airfoil are identical. The leading edge radius is 1.8% (4.23 mm). Figure 1 shows the two–dimensional shape of the airfoils.

(a) Original SD7003–shaped airfoil geometry (tripping device included), used for the non–porous reference airfoil

(b) Slightly modified SD7003–shaped airfoil geometry with an increased trailing edge thickness, used for the porous airfoils

Figure 1. Comparison of the two airfoil designs, both having the same chord length c_l = 235 mm

The porous airfoils are characterized by their air flow resistivity r, which can be calculated according to Darcy's law[10] based on the pressure difference Δp_s across a cylindrical porous sample of cross–sectional area A_s and thickness d_s and the product of the velocity u_s of a static fluid flow through the sample:

$$r = \frac{\Delta p_s}{u_s \cdot d_s}. \tag{2}$$

The air flow resistivity of the porous materials was measured according to ISO 9053[11] and is given in Table 1 for all airfoils of the present study, which are the same as used for the investigation of trailing edge noise by Geyer et al.[7]

II.B. Wind tunnel

For the investigation of the generation of leading edge noise, a circular nozzle with a diameter of 0.2 m was used. With this nozzle, the open jet aeroacoustic wind tunnel has a very low turbulence in the core jet, which is in the order of 0.1% directly in front of the nozzle at a flow speed of 20 m/s and a very low wind tunnel self noise, with an overall sound pressure level below 60 dB(A) for flow speeds up to 50 m/s. Sarradj et al.[12] give additional information on the aeroacoustic wind tunnel used for the present study.

During acoustic measurements, the test section in front of the nozzle is surrounded by a cabin whose floor and side walls are equipped with a porous absorber, thus providing a nearly anechoic acoustic environment for frequencies above 500 Hz, while the planar microphone array used for the acoustic measurements forms the ceiling. The wall on the opposite side of the nozzle is open.

Figure 2(a) shows a photograph of the setup, including the nozzle (which is additionally equipped with an open–porous foam to avoid sound reflection effects at the nozzle), the non–porous reference airfoil, a turbulence grid and the microphone array at the ceiling of the cabin. A schematic of the measurement setup is given in Figure 2(b). Note that throughout the present paper, the x-coordinate refers to the streamwise (chordwise) direction, the y-coordinate refers to the lateral (spanwise) direction and the z-coordinate refers to the vertical direction.

Table 1. Airfoils used in the experiments

No.	Name	Material	r [Pa s/m^2]
1	Reference	non–porous	∞
2	M&K felt, 0.36 g/cm^3	woolen felt	506,400
3	Porex	synthetic foam	316,500
4	M&K felt, 0.22 g/cm^3	woolen felt	164,800
5	Needlona felt, SO 2002	synthetic felt	130,200
6	ArmaFoam Sound	elastomer foam	112,100
7	Needlona felt, WO–PE 1958	woolen / synthetic felt	40,100
8	Arpro Porous 4025	expanded polypropylene foam	23,100
9	Reapor	porous glass granulate	16,500
10	Basotect	melamine resin–foam	9,800
11	Recemat	metal foam	8,200
12	Balzer RG 3550	polyurethane foam	4,400
13	Panacell 90 ppi	polyurethane foam	4,000
14	Panacell 60 ppi	polyurethane foam	3,600
15	M–Pore PU 45 ppi	polyurethane foam	1,500
16	M–Pore Al 45 ppi	metal foam	1,000
17	Panacell 45 ppi	polyurethane foam	700

II.C. Turbulence grids

Noticeable noise is generated at the leading edge of an airfoil if the incoming flow contains considerable turbulence. Possible means to generate this inflow turbulence are the use of cylinders or grids. In the present study, the turbulence was generated by commercially available perforated plates and square mesh grids. The parameters defining the geometry of the grids are illustrated in Figure 3. Additionally, the parameter t describes the thickness of the grids.

Based on these parameters, the grid porosity, as the ratio of the effective open area of the grid to the total area, can be calculated as[13]

$$\beta = \left(1 - \frac{a}{M}\right)^2 = \left(1 - \frac{a}{a+b}\right)^2 . \tag{3}$$

Prior hot–wire measurements were conducted[14] in order to select a set of three grids out of a total of twelve available turbulence grids. The aim of these measurements was to identify those grids that generate a maximum turbulence, and hence a maximum turbulence intensity

$$Tu = \frac{\sqrt{\overline{u^2}}}{U}, \tag{4}$$

at the position of the airfoil leading edge. In Equation 4, $\sqrt{\overline{u^2}}$ is the root mean square of the turbulent velocity fluctuations, which is equal in each direction for locally isotropic turbulence, and U is the mean flow speed. The three turbulence grids that were finally chosen for the leading edge noise measurements are given in Table 2.

Table 2. Turbulence grids used in the experiments, grid parameters according to Figure 3 for perforated plates with square holes (*PPS*) and square mesh grids with round bars (*SMR*). The grid porosity β is calculated according to Equation (3).

Abbr.	description	M [mm]	a [mm]	t [mm]	β
PPS 12/2	perforated plate with square holes	12 (mesh width)	2 (bar width)	1	0.69
PPS 14/4	perforated plate with square holes	14 (mesh width)	4 (bar width)	1	0.51
SMR 5/1	square mesh grid with round bars	5 (mesh width)	1 (rod diameter)	2	0.64

Another common parameter to characterize a turbulent flow is the integral length scale Λ of the turbulence, which is a measure for the characteristic size of turbulent eddies within the flow. The definition of

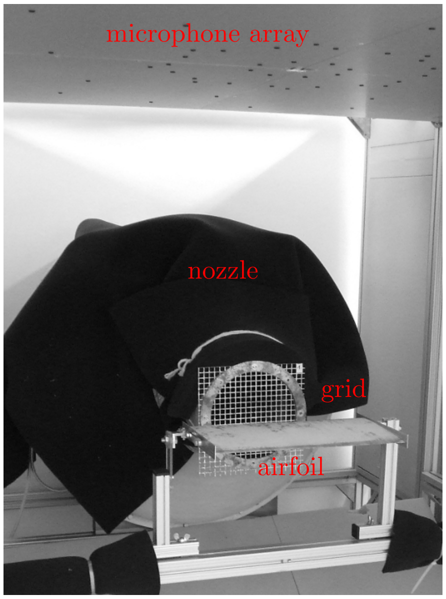

(a) Photograph of the measurement setup

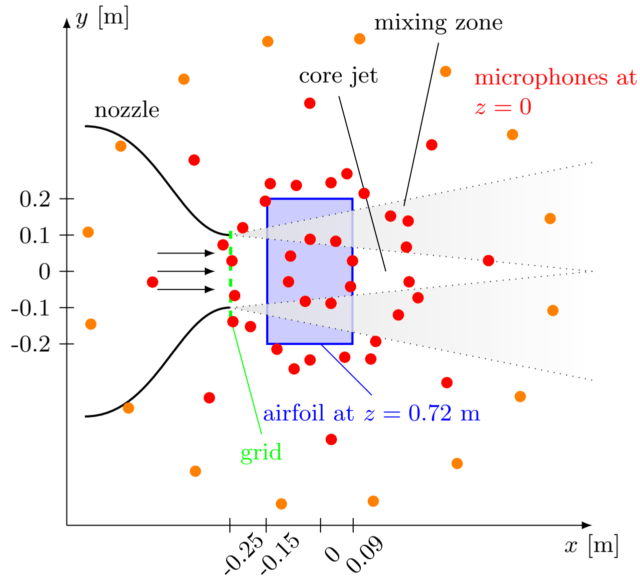

(b) Schematic display of the measurement setup (top view)

Figure 2. Measurement setup used for the investigation of the leading edge noise generated by porous airfoils

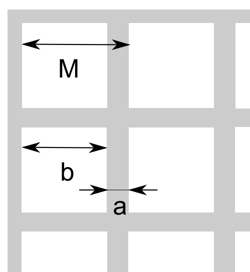

Figure 3. Definition of grid parameters mesh width M, bar width or rod diameter a and hole diameter b

such a scale is based on the hypothesis that the shape of a turbulent eddy can be assumed to be constant when its lifespan is at least one order of magnitude larger than the time the eddy needs to move past the measurement point (Taylors "frozen turbulence" hypothesis[15]).

In the present study, the integral length scale was determined using the autocorrelation method based on the measurements with a single hot–wire probe only, according to

$$\Lambda = U \int_0^\infty R(\tau) d\tau. \tag{5}$$

The term $R(\tau)$ denotes the autocorrelation of the velocity time series $u(t)$, with the offset (the constant flow speed U) removed,

$$R(\tau) = \frac{\overline{u(t) \cdot u(t-\tau)}}{\overline{u^2}}, \tag{6}$$

where the overline denotes the time mean.

The autocorrelation function $R(\tau)$ may also be calculated in the frequency domain instead of the time domain, since according to the Wiener-Khinchine theorem[16] the autocorrelation function in the time domain corresponds to the autospectral density in the frequency domain. The calculation in the frequency domain results in a noticeable reduction of computation time and easily allows for additional filtering of the signal. Thus, the data were transformed into the frequency domain by using a Fast Fourier Transformation (FFT) on 999 blocks with a size of 4,096 samples. The resulting frequency domain data were averaged over all blocks and the autospectral density was calculated. The result was then transformed back into the time domain by using the Inverse Fast Fourier Transformation (IFFT). The integration in Equation (5) was not performed over the entire available time domain, but from zero to the first zero-crossing as proposed by Katul and Parlange[17] and recommended by O'Neill et al.[18]

For the intended acoustic experiments on airfoil leading edge noise by using grids to generate the inflow turbulence, basically two needs have to be met: On the one hand, for the essential separation of noise generated by the grid itself from the noise sources located at the airfoil leading edge using microphone array technology it is advantageous when the distance between the grid and the airfoil leading edge is not too small. On the other hand, the turbulence intensity Tu decreases with increasing distance from the grid. Therefore, the distance between the grid and the leading edge should not be too large, because otherwise the turbulence intensity at the position of the leading edge is lower and thus less leading edge noise may be generated.

Finally, a distance of 0.1 m between the grids and the airfoil leading edge was chosen at which the grids generate turbulence with an intensity of approximately 9.4% (PPS 14/4), 7.4% (PPS 12/2-1) and 3.2% (SMR 5/1).

It is known from different experimental studies[13,19] that grid generated turbulence can only be viewed as isotropic and homogeneous for distances approximately larger than ten mesh widths from the grid. In order to meet this condition in the present experiments, the airfoil leading edge would have to be located approximately ten times the mesh size of the PPS 14/4 grid, and hence 0.14 m from the grid. This has not been done, since according to the results from the prior hot–wire measurements the turbulence intensity at this distance would be below 5% for two of the three grids. Turbulence intensities above 5% were desired for the present experiments in order to generate a measurable amount of leading edge noise and, more important, to examine the influence of the turbulence intensity on the generation of leading edge noise. The chosen distance of 0.1 m between grid and airfoil leading edge therefore poses the problem that the turbulence at the position of the leading edge cannot be assumed to be fully isotropic and homogeneous. Measurements using multi–wire probes would be necessary in order to obtain the velocity components in each direction, which could then be used to calculate all components of the turbulence intensity and the integral length scale separately.

In general, grid generated turbulence deserves further study. It is, however, beyond the scope of the present paper.

II.D. Determination of the flow parameters

Besides the information on the turbulence generated by the grids when no airfoil is subject to the flow, it is of relevance for the present study if the presence of the airfoils has an influence on the flow field directly upstream of the leading edge. This is especially of interest for airfoils with different air flow resistivities r compared to the non–porous reference airfoil.

To this end, Figure 4 shows the root–mean–square of the turbulent velocity fluctuations $\sqrt{\overline{u^2}}$ and the mean flow velocity U measured upstream of three different airfoils (the non–porous reference airfoil, the airfoil made of M–Pore Al 45 ppi, r = 1,000 Pa s/m^2, and the airfoil made of Recemat, r = 8,200 Pa s/m^2) for two of the turbulence grids. The parameters were calculated based on Equation (4) and (5), and hence based on the assumption of locally isotropic turbulence, at each streamwise position.

A multi–channel constant temperature anemometry (CTA) measurement system with a right-angled single–wire probe (Dantec 55P14) was used for these measurements. The probe was positioned using a 3D traverse system with a minimum step size of 0.1 mm. The measurement system contains a 10 kHz low-pass filter. The velocity time series were recorded with a sample frequency of 25.6 kHz and a measurement duration of 10 s using a 24 Bit National Instruments data acquisition system. To eliminate the influence of possible vibrations of the hot–wire probe after each step of the traverse system, the first second of each measurement was omitted, leaving 230,400 samples to be analyzed. An additional 10 Hz high-pass filter was implemented in the analysis software in order to eliminate the offset voltage. All hot–wire calibrations were performed with the velocity calibration method using a Pitot tube.

The measurements were performed in a plane normal to the flow at a distance of 7 mm upstream of the leading edge of the airfoils. This was the smallest possible distance due to the length of the prongs of the hot–wire probe.

It can be seen from Figure 4 that the material only has a small influence on the flow parameters upstream of the leading edge. For the three examined airfoils, there are only minor differences in the rms velocity,

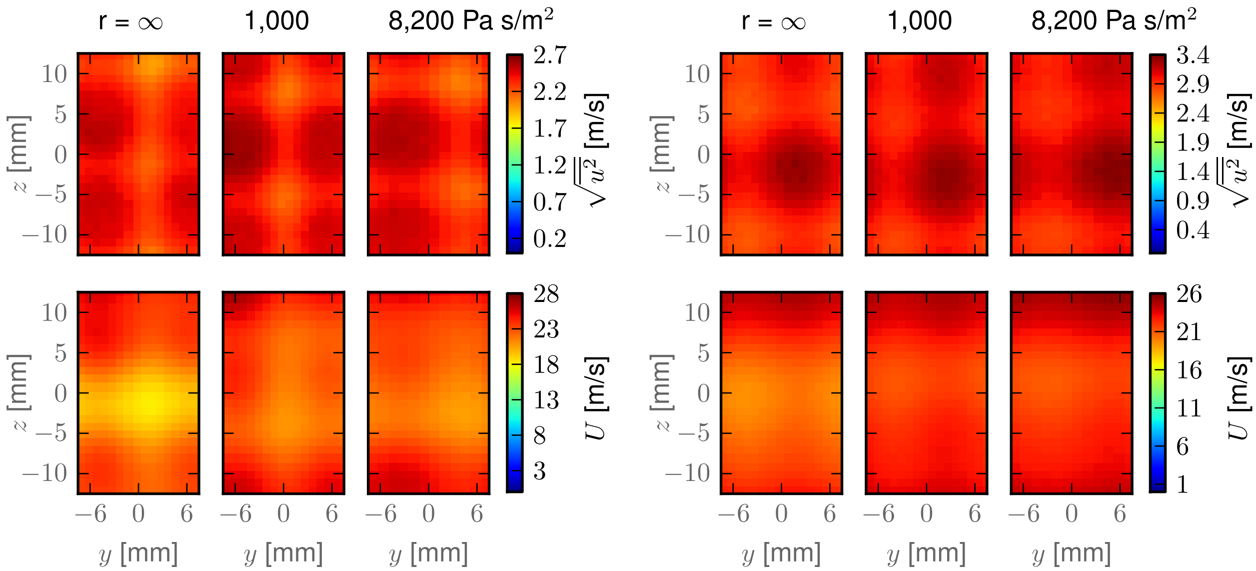

(a) PPS 12/2 turbulence grid (b) PPS 14/4 turbulence grid

Figure 4. Results of preliminary CTA–measurements to determine the possible influence of the presence of the airfoil on the flow parameters directly upstream of the leading edge, nominal flow speed U_0 = 30 m/s

the mean flow speed and the turbulence intensity. For example, the maximum difference of the flow speed is 1.4 m/s for the PPS 12/2 grid and 0.7 m/s for the PPS 14/4 grid (corresponding to a difference of 5.4% and 2.8% relative to the flow speed measured upstream of the reference airfoil), and the maximum difference of the turbulence intensity is 1.0% and 1.4% (corresponding to differences of 8.1% and 8.6% relative to the turbulence intensity measured upstream of the reference airfoil), respectively.

It is also visible from Figure 4 that, as suspected, the flow field and the turbulence generated at a distance of 0.1 m from the grids is not homogeneous, but shows differences which are correlated to the geometry of the grids. At regions that correspond to holes in the grid, the rms velocity and also the turbulence intensity are larger than in the "shadowed" region behind the bars of the grid. However, Figure 4 also shows that the turbulence at a distance of 0.1 m from the two perforated plates is relatively close to homogeneity.

Based on these preliminary results it was decided to measure the characteristic parameters of the turbulent inflow that are assumed to have an influence on the generation of noise at the airfoil leading edge (the mean velocity U, the turbulence intensity Tu and the integral length scale Λ) for only one airfoil, the non–porous reference airfoil, instead of performing individual hot–wire measurements for each airfoil from Table 1. Hence, for each of the three grids from Table 2 and for each flow speed U_0 CTA measurements were performed 7 mm upstream of the leading edge of the non–porous airfoil in a plane normal to the flow, using a right-angled single–wire probe. In order to characterize the flow directly in front of the leading edge as near as possible to the stagnation point, the plane should have a small vertical extent (normal to the airfoil) only, but a somewhat larger spanwise extent to allow for the averaging over the varying flow parameters caused by the meshes of the grid. The chosen plane has a height (vertical extent in z-direction) of 5 mm and a width (spanwise extent in y-direction) of 50 mm. Regarding the number of measurements within this plane, it should on the one hand be sufficiently large to result in a representative description of the turbulent inflow, and hence the plane should span an area including more than one mesh. On the other hand, it was attempted to keep the number of measurements small to save measurement time. The resulting 33 hot–wire measurement positions within the plane are indicated in Figure 5. The single measurement locations were chosen to result in a more or less random distribution, and periodic increments were avoided.

The reason to conduct the measurements in a plane instead of measuring at one single point only is the variation of the flow parameters mentioned above. In order to obtain a more significant characterization of the turbulent inflow, the parameters are averaged over the complete plane. Figure 6 shows the resulting parameters U, Tu and Λ of the turbulent inflow including the standard deviation as measured inside the plane shown in Figure 5 upstream of the non–porous reference airfoil.

The mean flow velocity U at the approximate position of the leading edge is a constant fraction of U_0 for

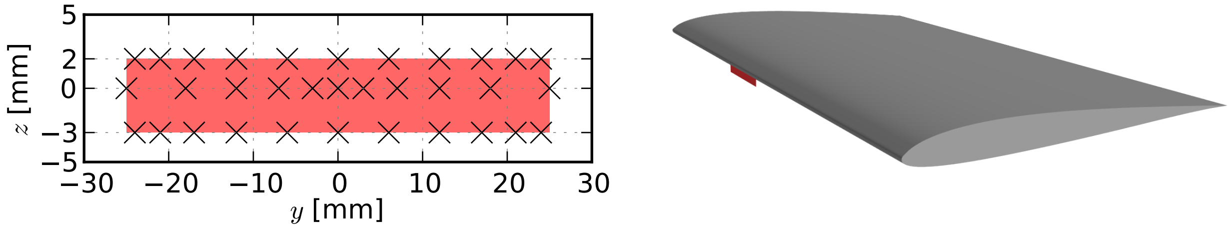

Figure 5. Hot–wire measurement locations used to calculate the flow parameters U, Tu and Λ upstream of the leading edge of the airfoils (the plane is located 7 mm upstream of the leading edge, normal to the direction of the flow; the origin refers to the leading edge position at midspan)

all grids, with a small standard deviation only. This is due to the presence of the airfoil and the location of the measurement positions near the stagnation point. The turbulence intensity Tu generated by the grids is nearly constant at all nominal flow speeds U_0, again with a reasonable standard deviation. But while the two perforated plates (PPS 12/2 and PPS 14/4) produce good results with reasonable standard deviations for the integral length scale Λ, the integral length scale of the turbulence generated by the square mesh grid with round bars (SMR 5/1) is noticeable different from that measured for the two other grids. At nominal flow speeds below 15 m/s the integral length scale is in the order of that measured for the perforated plates, with a relatively small standard deviation. With increasing flow speed up to about 20 m/s, Λ increases strongly. For further increasing flow speeds, the mean value of the integral length scale keeps approximately constant, but shows a very large standard deviation. The reason for this sudden increase of the mean value and, moreover, for the relatively large standard deviation, is not clear (particularly since the other parameters U and Tu do not show such noticeable behaviour). Interestingly, the SMR 5/1 grid is also the grid for which the condition that the measurement distance should be larger than approximately ten mesh widths[13] was met, so that the turbulence can be taken to be locally isotropic and homogeneous. The cause of the differences may be connected to the different type of grid and the associated grid parameters, specifically the round bars. It may be caused by a change in the flow regime around the circular bars. The according Reynolds number based on bar diameter, $Re = U_0 \cdot a/\nu$, is approximately 660 at a flow speed of 10 m/s and 1330 at 20 m/s when using a kinematic viscosity $\nu = 1.5 \cdot 10^{-5}$ m^{2}s^{-1}. A circular cylinder generates a street of regularly spaced vortices that have laminar cores for Reynolds numbers based on cylinder diameter between approximately 55 and 400, while for Reynolds numbers above 400 (and up to 200.000) the vortex street remains regular, but the cores of the vortices become turbulent.[20] Thus, the change in integral length scale may be related to the transition of the laminar cores to turbulent cores. Additionally, the aspect ratio (as the ratio of cylinder height to diameter) is 4, and hence very small only, so that the generated vortex street may be unstable. The experiments conducted by Holle[21] give evidence that for short cylinders the generation of vortices is different from that of longer cylinders, since aeolian tones, as a direct consequence of a regular vortex street, were only observed for cylinders with a certain minimum length. Due to the relatively short measurement duration of 10 s, the recorded data for the SMR 5/1 grid (leading to the curve shown in Figure 6(c)) may not be statistically representative to fully capture such an unstable process, which would then result in a large standard deviation.

II.E. Microphone array and data processing

The acoustic measurements were performed using a planar microphone array, which consists of 56 1/4" microphone capsules flush–mounted into a 1.5 m × 1.5 m aluminum plate, resulting in an aperture of 1.3 m. The position of each microphone is indicated in Figure 2(b). The array is mounted out of the flow, at a distance of 0.72 m above the airfoil. The streamwise position of the airfoil leading edge in array coordinates is x = -0.147 m.

The acoustic measurements were performed with a sample rate of 51.2 kHz and a measurement duration of 40 s, leading to a total of 2,048,000 samples per measurement. The raw data were stored and then further processed using advanced beamforming algorithms. In a first step, the data were blockwise transformed using an FFT with a Hanning window, each block having a size of 4,096 samples. This leads to a frequency spacing of 12.5 Hz. The cross spectral matrix was calculated for each block and averaged over a total of 999 blocks with 50% overlap.

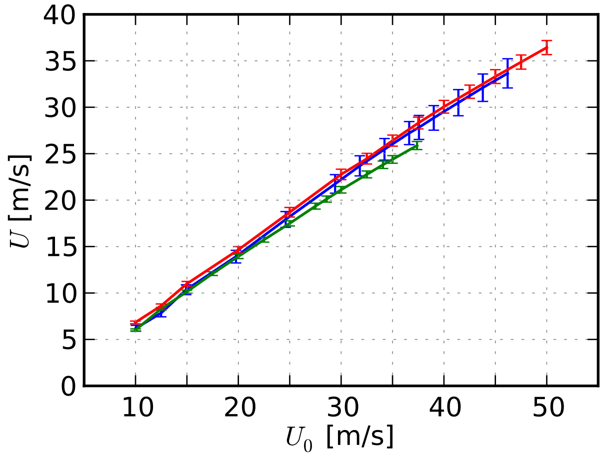

(a) Mean flow velocity U

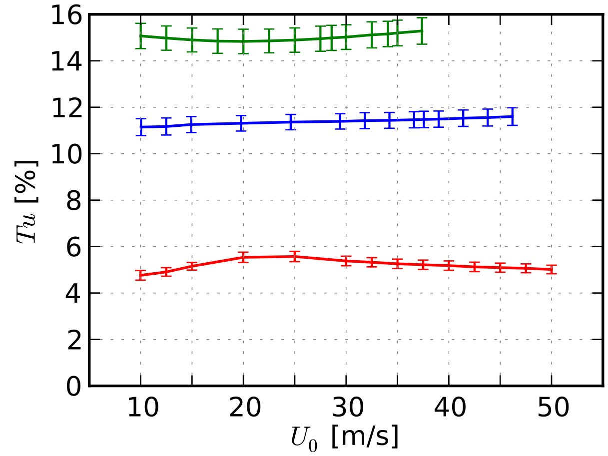

(b) Turbulence intensity Tu according to Equation (4)

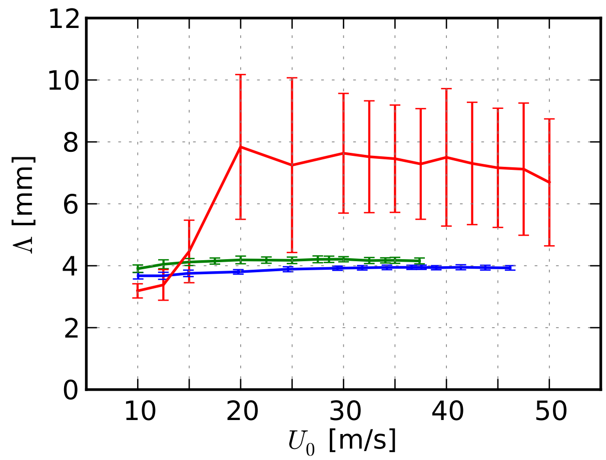

(c) Integral length scale Λ according to Equation (5)

Figure 6. Parameters of the turbulent inflow, measured in a plane according to Figure 5 7 mm upstream of the leading edge of the non–porous reference airfoil, as a function of the nominal flow speed U_0 (turbulence grids: — PPS 12/2, — PPS 14/4, — SMR 5/1)

In conventional beamforming, the noise sources located by the beamforming algorithm are usually mapped onto a two–dimensional plane (the result is called a sound map). In the case of a planar microphone array, this plane is most often orientated parallel to the array and located in the array focus point. The source region is represented by a two–dimensional grid, and potential noise sources are assumed to be located at the grid points. For the present investigation, a more advanced approach was used. Thereby, potential sound sources are not assumed to be located within a planar source region only, but within a fully three–dimensional source region, represented by a three–dimensional grid. Noise sources may be located at each point of this three–dimensional grid. The result of this beamforming technique is a three–dimensional distribution of source locations and the respective contributions to the sound pressure level as measured at the center of the array.

Different deconvolution algorithms were considered for the investigation of airfoil leading edge noise, including the CLEAN–SC algorithm proposed by Sijtsma[22] and the orthogonal beamforming (OB) algorithm proposed by Sarradj.[23] The DAMAS algorithm developed by Brooks and Humphreys,[24] which is known to deliver good results in aeroacoustic tests especially at low frequencies, was not applied to the data since it was found to be computationally too expensive when used on a three–dimensional source region and the subsequent large number of grid points.

It was found in past trailing edge noise measurements[7] that the CLEAN–SC algorithm delivers good results especially at low frequencies, while at high frequencies the CLEAN–SC either fails to deliver correct amplitudes of the located noise sources or fails to locate noise sources at all. Since in the present study the low frequency range of the noise sources located at the airfoil leading edge is of main interest, it was decided to use the CLEAN–SC algorithm.

Figure 7 shows three–dimensional mappings of noise source locations (three–dimensional sound maps) with center frequencies of 2.5 kHz and 8 kHz, obtained with the CLEAN–SC algorithm, for a measurement on the reference airfoil positioned downstream of the turbulence grid PPS 12/2 at a nominal flow speed of approximately 45 m/s. Likewise, Figure 8 shows similar sound maps, but for the case without an airfoil but only the turbulence grid PPS 12/2 (the position of the airfoil is only indicated in Figure 8 to allow for comparison with Figure 7).

The figures illustrate that, when the airfoil is immersed in the turbulent flow generated by the grid, the resulting major noise sources at low frequencies (as in the 2.5 kHz third–octave band displayed) are located at the airfoil leading edge (Figure 7(a)), while at high frequencies (8 kHz third–octave band) the main sources are located at the turbulence grid (at x = -0.248 m, Figure 7(b)). Additionally, some minor noise sources are visible for the low frequency case which are located at the position where the wind tunnel shear layer interacts with the airfoil trailing edge. If no airfoil is present, noise sources are located at the turbulence grid in the complete range of frequencies examined, as can be seen from Figure 8.

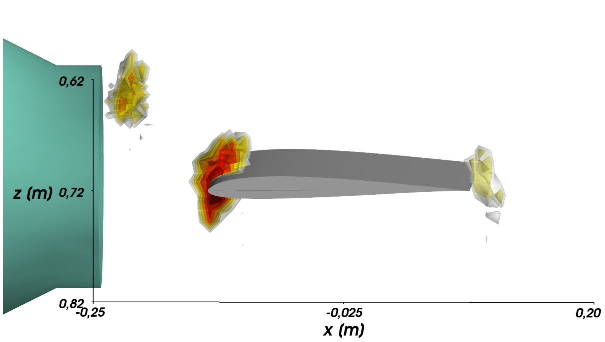

(a) f_c = 2.5 kHz, side view

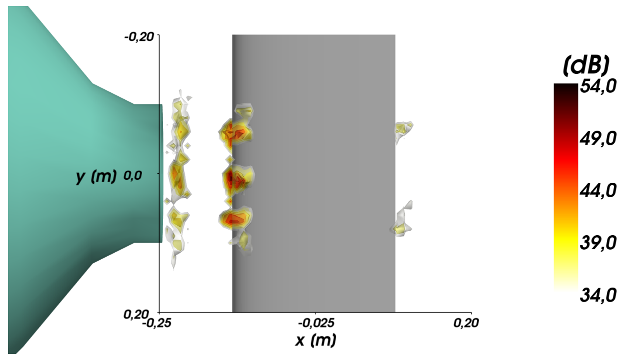

(b) f_c = 2.5 kHz, top view

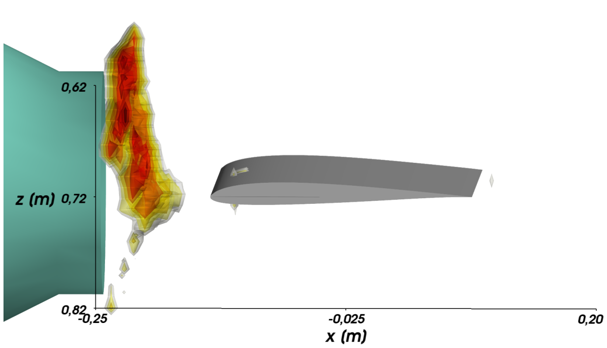

(c) f_c = 8 kHz, side view

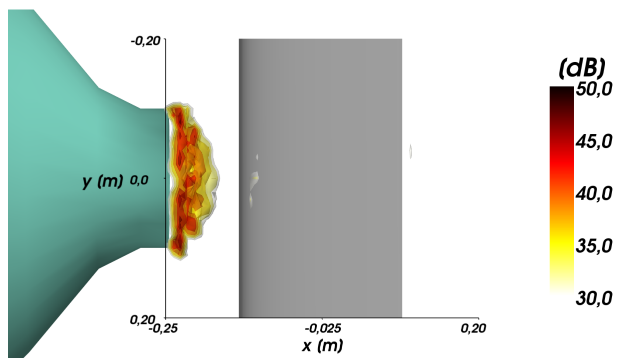

(d) f_c = 8 kHz, top view

Figure 7. Three–dimensional CLEAN–SC[22] sound maps obtained for the non–porous reference airfoil (view from above, flow from left to right, PPS 12/2 turbulence grid, $U_0 \approx$ 45 m/s)

To obtain spectra for the noise generated at the leading edge of the airfoils, the noise source contributions are integrated over a three–dimensional volume (as opposed a two–dimensional sector as used in two–dimensional beamforming) that contains only the airfoil leading edge, but no other potential noise source location. Major noise sources that are excluded from the integration are noise sources located at the turbulence grid (grid self noise), noise sources that are generated due to the impingement of the wind tunnel shear layer on the airfoil leading edge and surface and noise sources located at the airfoil trailing edge. The chosen volume, shown in Figure 9, has an extent of 0.1 m in the streamwise direction (-0.167 m $\leq x \leq$ -0.067 m), 0.12 m in the spanwise direction (-0.06 m $\leq y \leq$ 0.06 m) and 0.12 m in the vertical direction (0.66 m $\leq y \leq$ 0.78 m). The resulting distance between the turbulence grid and the upstream boundary of the leading edge noise sector is 0.08 m.

For reasons of comparison, the spectra resulting from the integration over the leading edge sector for the

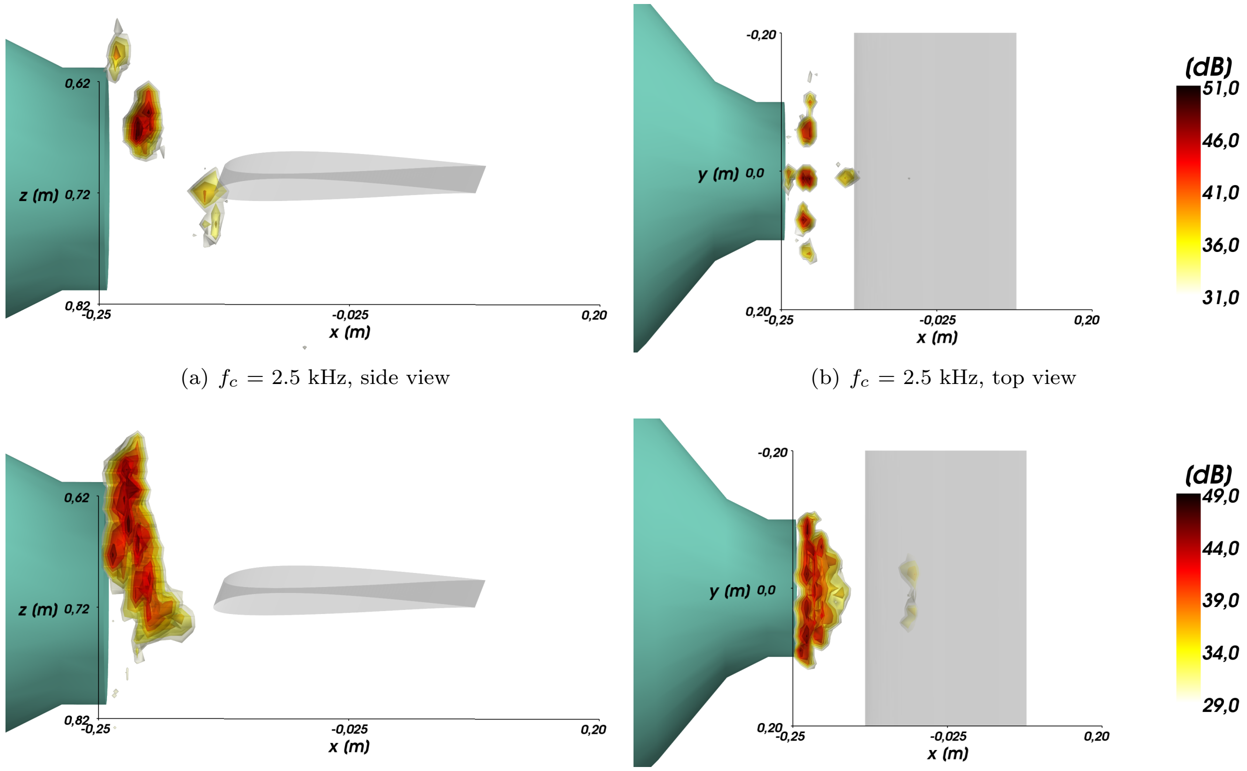

(a) $f_c = 2.5$ kHz, side view (b) $f_c = 2.5$ kHz, top view

(c) $f_c = 8$ kHz, side view (d) $f_c = 8$ kHz, top view

Figure 8. Three–dimensional CLEAN–SC[22] sound maps obtained for the empty test section (position of the airfoil is indicated to enable comparison with Figure 7) (view from above, flow from left to right, PPS 12/2 turbulence grid, $U_0 \approx 45$ m/s)

empty test section without airfoil will also be considered in the analysis of the measurements, although the results are physically not meaningful since no distinct noise sources are located within this volume. However, they will be included as an approximate measure of the background noise.

The examination of the three–dimensional sound maps indicated that care has to be taken regarding the frequency range to be analyzed, since at high frequencies background noise may be present within the airfoil leading edge noise sector. To avoid the contribution of background noise to the leading edge noise, the sound pressure levels measured within the leading edge noise sector for the empty test section cases will have to be considered when discussing the results. If necessary, the high frequency noise levels at which grid noise may be dominant have to be discarded.

Besides the potential upper frequency limit due to the presence of grid noise, acoustic measurements on airfoil edge noise, referring to either leading edge or trailing edge, are usually constricted to the acoustic frequency range at which the corresponding wavelengths are small compared to the chord length of the airfoil. In this case the non–compactness condition,[25]

$$\lambda < c_l, \tag{7}$$

is met, which in the present experimental study holds true for frequencies approximately equal to and larger than 1.5 kHz. Above this frequency, the noise generated by the airfoil leading edge can clearly be considered as separated from the noise generated at its trailing edge. Nevertheless, the use of microphone array technology and advanced deconvolution beamforming techniques should allow for the identification and separation of edge noise sources at frequencies somewhat below that limit. The lowest third–octave band considered in the present analysis has a center frequency of 1 kHz.

No correction for the refraction of sound at the shear layer was applied due to the fact that the exact shape and thickness of the conical shear layer of the wind tunnel is not known. Common correction procedures, like the method developed by Amiet and Schlinker,[26,27] are based on the assumption of a cylindrical shear layer of constant thickness. Such procedures do not seem appropriate for the present measurement setup

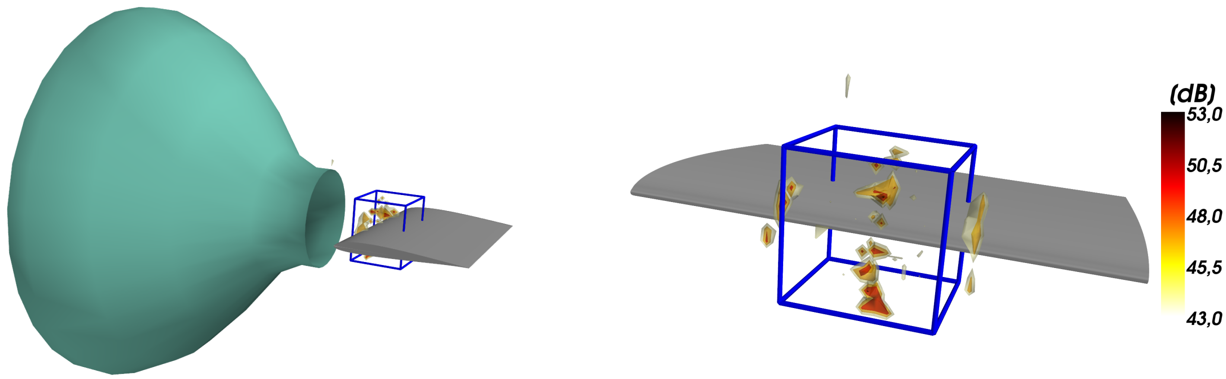

(a) Wind tunnel nozzle and airfoil (turbulence grid not included in the figure)

(b) Detailed view of integration volume

Figure 9. Airfoil leading edge noise volume (sample sound map: non–porous reference airfoil, PPS 12/2 turbulence grid, $U_0 \approx$ 45 m/s, CLEAN–SC, 2 kHz third–octave band)

and the necessary effort for the implementation does not seem justified. Additionally, the distance between the noise source locations at the leading edge and the shear layer is relatively small (in the order of one half nozzle diameter, 0.1 m) compared to the distance of 0.72 m between the leading edge and the microphone array center, which results in only small deviations of the noise source locations due to refraction at the shear layer.

Finally, the measured sound pressure levels were corrected for the reflection at the microphone array flat plate by subtracting 6 dB.

III. Results and discussion

Measurements were conducted at zero angle of attack for 14 flow speeds between 10 m/s and 50 m/s for each turbulence grid from Table 2 and for each of the airfoils from Table 1, including measurements with an empty test section (no airfoil) for means of comparison. This lead to a total of about 760 single measurements and more than 340 GByte of raw data.

III.A. Sound maps

As a first result, Figure 10 shows sample third–octave band sound maps for three porous airfoils and the reference airfoil for a center frequency of 2 kHz, and hence for the frequency domain where the airfoil leading edge is clearly the dominating noise source.

It is clearly visible that the noise generated at the leading edge of the porous airfoils is below that generated at the leading edge of the non–porous reference airfoil. This includes both the two lateral sources due to the interaction of the wind tunnel shear layer with the leading edge as well as the source due to the interaction of the leading edge with the grid generated turbulence, located approximately at midspan.

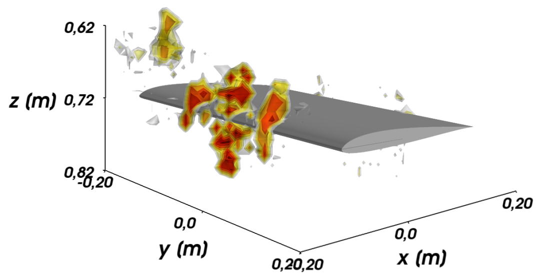

(a) Non–porous reference airfoil, $r = \infty$

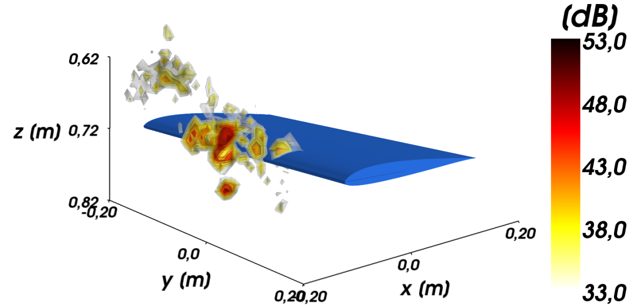

(b) Porous airfoil made of Needlona felt, r = 40,100 Pa s/m^2

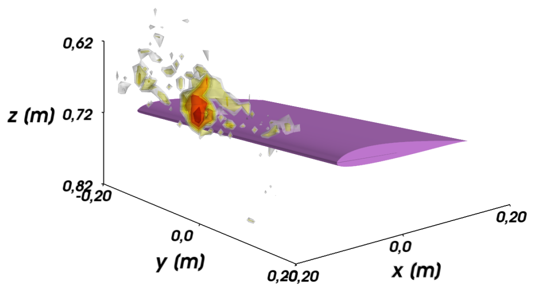

(c) Porous airfoil made of Basotect, r = 9,800 Pa s/m^2

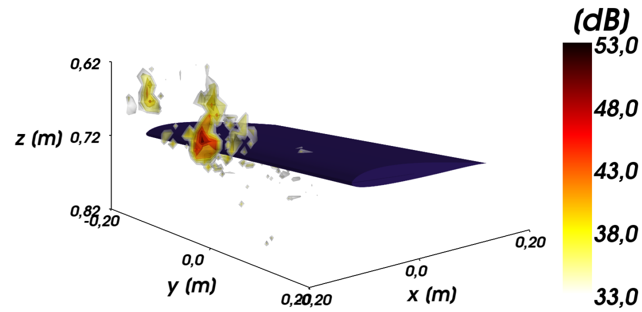

(d) Porous airfoil made of M–Pore Al 45 ppi, r = 1,000 Pa s/m^2

Figure 10. Three–dimensional third–octave band sound maps, CLEAN–SC beamforming algorithm, center frequency 2 kHz (Note that all sound maps are scaled to the same maximum level of 53 dB measured for the reference airfoil.)

III.B. Third–octave band sound pressure level spectra

Third–octave band sound pressure level spectra that were obtained through integration of the three–dimensional sound maps over the leading edge noise volume shown in Figure 9 for one flow speed are shown in Figure 11(a) for the first turbulence grid from Table 2, in Figure 11(b) for the second grid and in Figure 11(c) for the third grid.

Additionally, each figure contains the leading edge noise spectrum calculated using the Amiet model[2] as given by Equation (1). The input parameters are the spanwise extent of the chosen leading edge noise sector as shown in Figure 9, the distance between the array center and the leading edge at midspan, the flow speed U_0, the root–mean–square of the turbulent velocity fluctuations, the integral length scale of the turbulence and the speed of sound. The good agreement between measurement and prediction serves as a basic validation for the present experimental study.

The measured spectra suggest the clear trend that porous airfoils with a very low air flow resistivity r lead to a larger noise reduction than airfoils with a higher air flow resistivity. The differences in sound pressure level measured at the leading edge of airfoils made of porous materials with air flow resistivities between approximately 700 Pa s/m^2 and 4,400 Pa s/m^2 (left column of Figure 11(a) through 11(c)) take maximum values in the order of 10 to 15 dB. In some cases, for example for the PPS 14/4 turbulence grid, the leading edge noise of the porous airfoils with low air flow resistivities is only slightly above the background noise. Medium air flow resistivities (center column of Figure 11(a) through 11(c)) result in maximum leading edge noise reductions of approximately 5 dB, while porous airfoils with high air flow resistivities (right column) only lead to a very small leading edge noise reduction or to no reduction at all. So, basically, the potential leading edge noise reduction increases with decreasing air flow resistivity of the porous airfoils, which is assumed to be caused by the (on average) larger pores of the materials with low air flow resistivities.

It is interesting that the spectra of the leading edge noise measured for the two perforated plates (PPS 12/2, Figure 11(a) and PPS 14/4, Figure 11(b)) show similar shapes, which is an indicator that the resulting leading edge noise spectrum essentially depends on the spectrum of the inflow turbulence. The spectrum measured for the reference airfoil downstream of the SMR 5/1 grid shows a sharp drop for frequencies below the 1.25 kHz third–octave band, which is not visible for the porous airfoils.

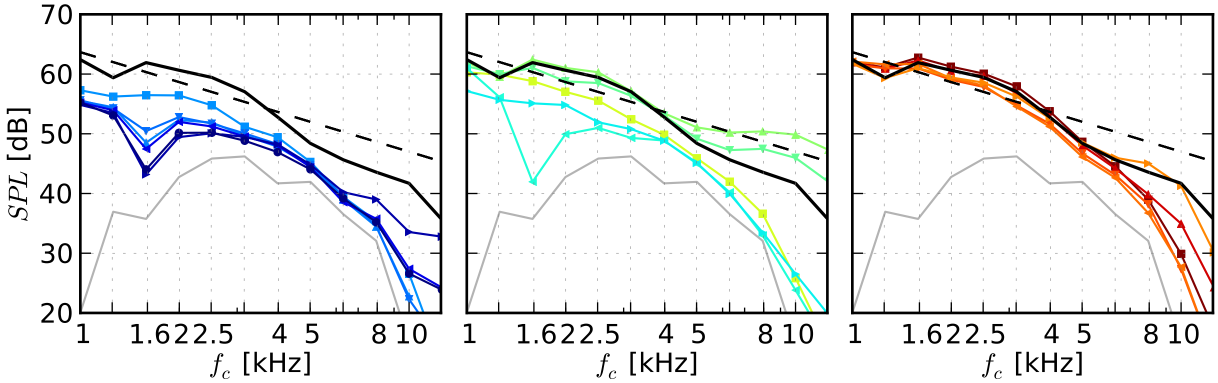

(a) PPS 12/2 turbulence grid, nominal flow speed $U_0 \approx 45$ m/s

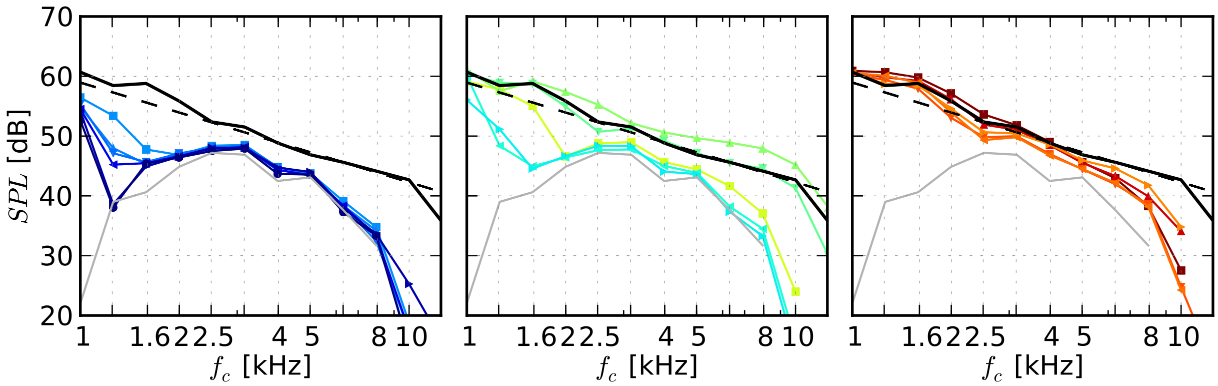

(b) PPS 14/4 turbulence grid, nominal flow speed $U_0 \approx 35$ m/s

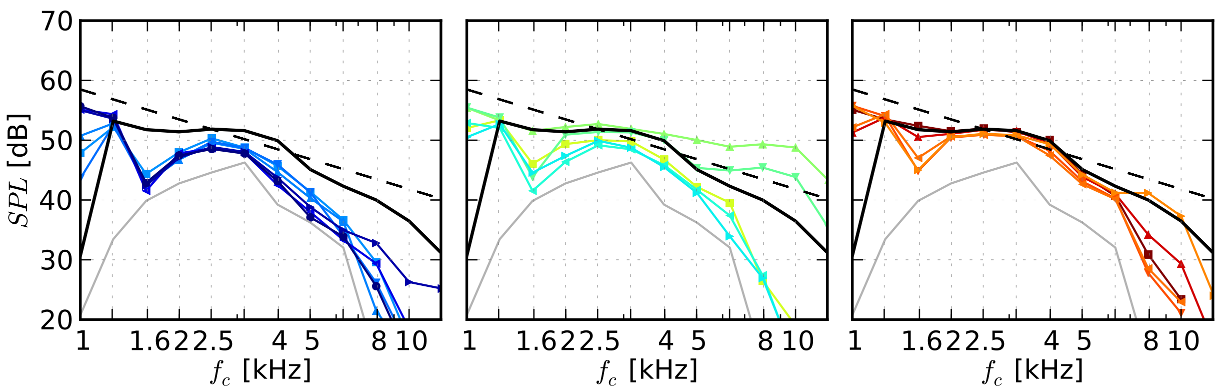

(c) SMR 5/1 turbulence grid, nominal flow speed $U_0 \approx 50$ m/s

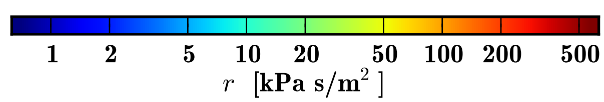

Figure 11. Leading edge noise third–octave band sound pressure levels, left: r = ■ 4,400, ▲ 4,000, ▼ 3,600, ◀ 1,500, ▶ 1,000, ● 700 Pa s/m^2, center: r = ■ 40,100, ▲ 23,100, ▼ 16,500, ◀ 9,800, ▶ 8,200 Pa s/m^2, right: r = ■ 506,400, ▲ 316,500, ▼ 164,800, ◀ 130,200, ▶ 112,100 Pa s/m^2, — reference airfoil ($r = \infty$), — empty test section, – – Amiet model[2] according to Equation (1)

III.C. Scaled third–octave band sound pressure level spectra

In order to enable a comparison of the measured leading edge noise for more than one flow speed, the third–octave band sound pressure levels are presented as a function of a Strouhal number. Therefore, in a first step an appropriate Strouhal number has to be chosen, which may either contain a dimension characteristic for the airfoil, as the maximum thickness or the chord length, or a dimension characteristic for the turbulence, as the integral length scale of the turbulence or a grid parameter like the bar width or rod diameter. Additionally, the required velocity may be the mean flow speed U measured upstream of the leading edge or the nominal flow speed U_0.

In accordance to the experimental study by Oerlemans and Migliore,[28,29] who use a Strouhal number based on airfoil chord length and flow speed as measured in the wind tunnel without grid (corresponding to the nominal flow speed U_0 in the present experiments) for the presentation of their inflow turbulence noise spectra, in a first approach the measured airfoil leading edge noise will be presented as a function of the Strouhal number based on airfoil chord length and nominal flow speed, $Sr = f_c \cdot c_l / U_0$. Furthermore, the measured leading edge noise levels will be scaled with the flow speed using the common approach

$$SPL_{\text{scaled}} = SPL - 10 \cdot \log \left(\frac{U_0}{1\text{m/s}} \right)^n . \tag{8}$$

The use of different exponents n is reported in the literature, for example $n = 5$ (Amiet[2]), $n = 5.6$ (Fink[30]) or $n = 6$ (Oerlemans and Migliore[28,29]). As stated by Blake,[25] the noise from the leading edge at frequencies with wavelengths smaller than the chord length, and hence in the present case for third–octave bands below the 1.6 kHz third–octave band, has dipole character and should increase with U_0^6. For center frequencies above 1.6 kHz, the directivity is that of a half–baffled dipole due to the airfoil surface acting as a baffle, leading to a dependence on U_0^5.

In the present case, the best results were obtained when, in accordance to the results by Oerlemans and Migliore,[28,29] an exponent of $n = 6$ was used, although the differences between $n = 5$ and $n = 6$ are relatively small only. Figure 12 shows the resulting scaled leading edge noise third–octave band sound pressure levels as a function of the chord–based Strouhal number for all turbulence grids from Table 2. It was found that a better scaling could be achieved when a lower limit of the flow speed of 20 m/s for the PPS 12/2 and the SMR 5/1 grid and 25 m/s for the PPS 14/4 grid was chosen. As mentioned above, it is assumed that for lower flow speeds the grid generated vortex street is different, which leads to a change of the flow domain and becomes visible through a noticeable scattering of the scaled sound pressure levels. Additionally, background noise, most likely from the wind tunnel core jet, may become dominant at lower flow speeds. The upper frequency limit was 10 kHz for the measurements involving the perforated plates. For the measurements that included the SMR 5/1 grid, the third–octave bands with center frequencies above 6.3 kHz were omitted, since they were found to be contaminated by background noise, and third–octave band sound pressure levels below the 1.6 kHz third–octave band were omitted since they are clearly lower than the remaining sound pressure levels (as can be observed from Figure 11(c)) and were found to not scale properly.

The scaling with U_0^6 delivers good results for the non–porous reference airfoil, especially for the perforated plates (the scaled levels are more scattered for the square mesh grid, but still the exponent $n = 6$ was found to give satisfying results). In case of the porous airfoils, the chosen scaling approach seems to be a suitable initial guess, but it is not valid without restrictions. Good results are obtained especially for porous materials with high air flow resistivities, while for porous airfoils with low air flow resistivities the scaled sound pressure levels are more scattered.

Figure 12 again illustrates that porous airfoils with low air flow resistivities result in the highest leading edge noise reduction compared to the non–porous reference airfoil. At high Strouhal numbers, the leading edge noise of some of the porous airfoils with medium air flow resistivities exceeds that of the reference airfoil, the reason for which is not clear yet.

When using a Strouhal number depending on airfoil chord length and nominal flow speed as well as the nominal flow speed for the scaling, differences between the results for the different grids can be expected, since the differences in inflow turbulence are completely disregarded. This is clearly confirmed when comparing each diagram from Figure 12, which shows that the sound pressure levels measured with the PPS 14/4 grid (Figure 12(b)) are higher than the levels measured with the other two grids. This particular grid also resulted in the highest turbulence intensity, as was presented in Figure 6(b). The SMR 5/1 grid lead to the lowest turbulence intensity and the lowest leading edge noise levels (Figure 12(c)). A scaling approach that incorporates at least the turbulence intensity generated by each grid therefore seems to be very promising (as is, for example, incorporated in the model of Amiet[2]).

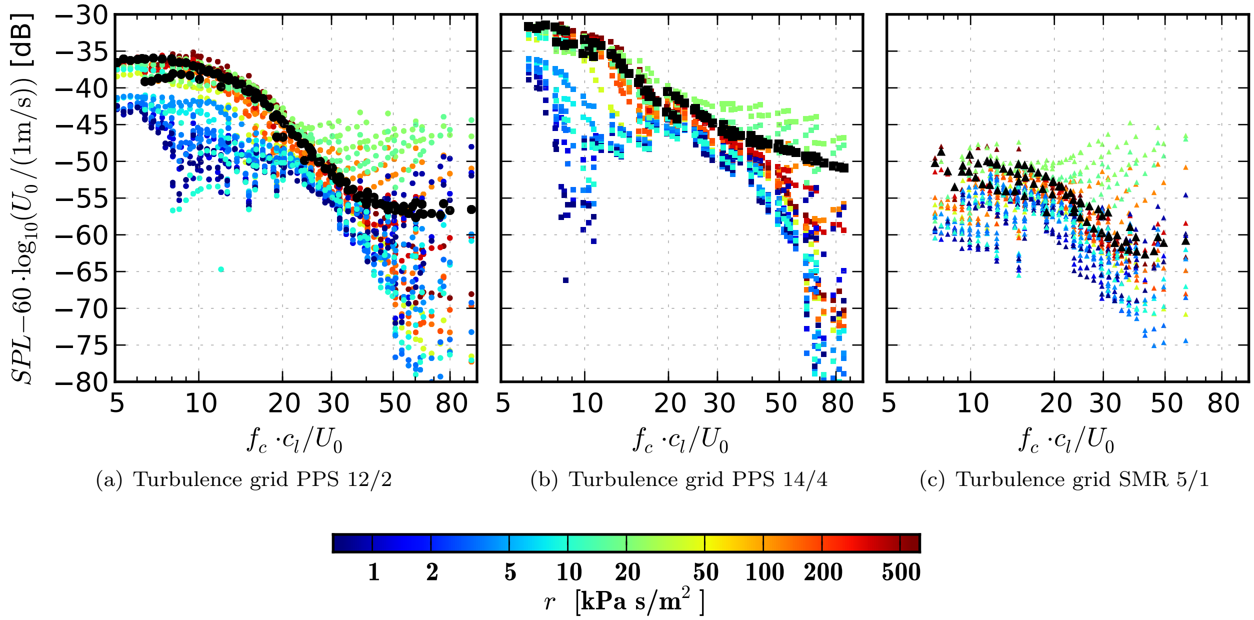

Figure 12. Leading edge noise third–octave band sound pressure levels as a function of the Strouhal number $f_c \cdot c_l/U_0$ for the three turbulence grids from Table 2

IV. Conclusions

The present paper describes an experimental study on the generation of noise at the leading edge of porous model airfoils compared to a non–porous reference airfoil.

The experiments were conducted in an open jet wind tunnel, and the inflow turbulence necessary for the generation of leading edge noise was generated by means of three different turbulence grids. The possible inhomogeneity of the turbulence generated by the grids may be a point of some concern, although it was tried to compensate for such effects by averaging the turbulence parameters over an area normal to the flow, located directly in front of the leading edge.

The acoustic measurements were performed with a planar 56 channel microphone array, positioned above the airfoils and out of flow. The acoustic data was further processed using the CLEAN–SC algorithm, but it was extended for a three–dimensional distribution of noise source locations. From the resulting three–dimensional sound maps, third–octave band sound pressure level spectra were obtained through integration over a three–dimensional volume that contains the leading edge noise sources but no other potential noise source locations, as for example the turbulence grid or the airfoil trailing edge.

The leading edge noise spectra measured for the non–porous reference airfoil are in good agreement with the predictions using the model developed by Amiet.[2] The results of the acoustic measurements show that the use of porous airfoils enables a noticeable reduction of leading edge noise, which is found to increase with decreasing air flow resistivity r. This is assumed to be caused by the relatively large pores in case of materials with a low air flow resistivity.

Acknowledgments

This research was sponsored by the *Deutsche Forschungsgemeinschaft* (DFG) in the priority program 1207, "Nature Inspired Fluid Mechanics", under the grant number SA 1502/1-3.

References

[1]S. Wagner, R. Bareiss, and G. Guidati. *Wind Turbine Noise*. Springer, 1996.

[2]R. K. Amiet. Acoustic radiation from an airfoil in a turbulent stream. *Journal of Sound and Vibration*, 41(4):407–420, February 1975.

[3]R. W. Paterson and R. K. Amiet. Acoustic radiation and surface pressure characteristics of an airfoil due to incident

turbulence. Technical report, NASA Contractor Report CR-2733, 1976.

[4]I. J. Sharland. Sources of noise in axial flow fans. *Journal of Sound and Vibration*, 3:302–322, 1964.

[5]S. Lee. Reduction of blade-vortex interaction noise through porous leading edge. *AIAA Journal*, 32:480 – 488, 1994.

[6]A.F. Tinetti, J.F. Kelly, R.H. Thomas, and S.X.S. Bauer. Reduction of wake-stator interaction noise using passive porosity. In *40th AIAA Aerospace Scienes Meeting and Exhibit, Reno, NV, AIAA paper 2002-1036*, 2002.

[7]T. Geyer, E. Sarradj, and C. Fritzsche. Measurement of the noise generation at the trailing edge of porous airfoils. *Experiments in Fluids*, 48 (2):291 – 308, 2010.

[8]T. Geyer, E. Sarradj, and C. Fritzsche. Porous airfoils: Noise reduction and boundary layer effects. *International Journal of Aeroacoustics*, 9 (6):787 – 820, 2010.

[9]M.S. Selig, J. Donovan, and D. Fraser. *Airfoils at Low Speeds*. SoarTech Aero Publications, 1989.

[10]A.E. Scheidegger. *The Physics of Flow through porous Media. Third Edition*. University of Toronto Press, 1974.

[11]ISO 9053. Acoustics – materials for acoustical applications – determination of airflow resistance. Technical report, International Organization for Standardization, 1993.

[12]E. Sarradj, C. Fritzsche, T. Geyer, and J. Giesler. Acoustic and aerodynamic design and characterization of a small-scale aeroacoustic wind tunnel. *Applied Acoustics*, 70:1073 – 1080, 2009.

[13]P. W. Roach. The generation of nearly isotropic turbulence by means of grids. *Journal of Heat and Fluid Flow*, 8 (2):82 – 92, 1987.

[14]M. Hobracht, E. Sarradj, and T. Geyer. Auslegung eines Turbulenzgitters für die Untersuchung des Vorderkantenschalls an einem Tragflügelprofil. In *Fortschritte der Akustik - DAGA 2011*, 2011.

[15]J. O. Hinze. *Turbulence. Second Edition*. McGraw-Hill, New York, 1975.

[16]J. S. Bendat and A. G. Piersol. *Random Data - Analysis and Measurement Procedures*. John Wiley & Sons, Inc., New York, 2000, Third Edition.

[17]G. G. Katul and M. B. Parlange. Analysis of land surface heat fluxes using the orthonormal wavelet approach. *Water Resources Research*, 31 (11):2743 – 2749, 1995.

[18]P. L. O'Neill, D. Nicolaides, D. Honnery, and J. Soria. Autocorrelation functions and the determination of integral length with reference to experimental and numerical data. In *15th Australasian Fluid Mechanics Conference*, 2004.

[19]Ö. Ertunç. *Experimental and Numerical Investigations of Axisymmetric Turbulence*. PhD thesis, Technical University Erlangen-Nürnberg, 2007.

[20]W.K. Blake. *Mechanics of Flow-Induced Sound and Vibration, Volume I: General Concepts and Elementary Sources*. Academic Press, Inc., 1986.

[21]W. Holle. Frequenz- und Schallstärkemessungen an Hiebtönen. *Akustische Zeitschrift*, 3 (6):321 – 331, 1938.

[22]P. Sijtsma. Clean based on spatial source coherence. In *13th AIAA/CEAS Aeroacoustics Conference, AIAA-paper 2007-3436*, 2007.

[23]E. Sarradj. A fast signal subspace approach for the determination of absolute levels from phased microphone array measurements. *Journal of Sound and Vibration*, 329:1553 – 1569, 2010.

[24]T. F. Brooks and W. M. Humphreys. A deconvolution approach for the mapping of acoustic sources (damas) determined from phased microphone arrays. In *10th AIAA/CEAS Aeroacoustics Conference, AIAA-paper 2004-2954*, 2004.

[25]W.K. Blake. *Mechanics of Flow-Induced Sound and Vibration, Volume II: Complex Flow-Structure Interactions*. Academic Press, Inc., 1986.

[26]R.K. Amiet. Refraction of sound by a shear layer. *Journal of Sound and Vibration*, 58:467 – 482, 1978.

[27]R. H. Schlinker and R. K. Amiet. Refraction and scattering of sound by a shear layer. Technical report, NASA, Langley Research Center under Contract NAS1-15339, 1980.

[28]S. Oerlemans. Wind tunnel aeroacoustic tests of six airfoils for use on small wind turbines. Technical report, National Renewable Energy Laboratory, NREL/SR-500-35339, August 2004.

[29]S. Oerlemans and P. Migliore. Aeroacoustic wind tunnel tests of wind turbine airfoils. In *10th AIAA/CEAS Aeroacoustics Conference, AIAA-Paper 2004-3042*, volume 3042, 2004.

[30]M. R. Fink. Investigation of scrubbing and impingement noise. Technical report, NASA Contractor Report CR-134762, 1975.